

# Research Journal of Pharmaceutical, Biological and Chemical Sciences

## Production and modification of PEO/PVDF Membranes Loaded with Silver Nitrate.

IS Elashmawi<sup>1,2,\*</sup>, and NH Hakeem<sup>1</sup>

<sup>1</sup>Department of spectroscopy, Physics division, National Research Center, Giza, Egypt.

<sup>2</sup>Department of Physics, Faculty of Science, Taibah University, Al-Ula, Saudia Arabia.

### ABSTRACT

Porous membranes of PEO/PVDF loaded with different concentrations of PEO and 10 wt.% of AgNO<sub>3</sub> nanoparticles were prepared. Structural, morphological and thermal properties of these membranes were studied. Most PVDF phases and compatibility with micropores were observed. Complexation between PVDF and PEO was significantly decreased with increasing of PEO content. FT-IR analysis revealed that some bands were disappeared with increasing of  $\gamma$ -phase of PVDF, this phase can be useful in electrical applications due to its polarizability since PVDF is piezoelectric polymer. UV-vis shows an exponential decay tail at low energy which indicates the presence of localized states in energy band gap. In SEM picture sponge-like pores are present structures. The porous size was distributed in range from 0.10 to 0.65  $\mu$ m. Increasing of PEO can decreased pore size of the membranes The values of both degree of crystallinity and melting temperature were decreased as the content of PEO increased which is attributed to homogeneity and miscibility between membranes composites.

**Keywords:** Polymeric membranes, Micropours, X-ray, SEM, DSC.

*\*Corresponding author*

## INTRODUCTION

Microporous structure of polymeric membranes is an important factor in membrane manufacturing processes. Membranes are prepared by casting method with solvent/nonsolvent technique. Porous of polymer membranes are formed when polyethylene oxide (PEO) is used as lower polymer concentration with other polymer. The exchange of major solvent and minor solvent in mixed phases of polymer blend continuously causes concentrated phase surrounding the porous within the blend [1, 2].

Polyvinylidene fluoride (PVDF) is used both in scientific area and technological applications [3, 4]. It has at least five different main phases,  $\alpha$ ,  $\beta$ ,  $\gamma$ ,  $\alpha_p$  and  $\gamma_p$  which are classified according to the conformation of chains and their molecular packing at different temperatures [5, 6]. PVDF is considered as fit membranes material, ultrafiltration and microfiltration [7] due to its excellent thermal stability as well as chemical resistance to aggressive reagents like organic solvents.

Although PEO is reported as a good material in some biomaterial and electrical applications such as drug delivery and sensitive sensors, etc [8, 9], it has a limited applications as a pure polymer. On the other hand, blending is often used to change some properties of polymeric materials.

Preparation of new membranes doped with dispersed inorganic particles like Ag in a polymeric matrix has been undertaken for many years. Ag has received the most attention because of its stability and availability [10]. Aravindan and and Vickraman were studied the (PVdF–HFP) membrane impregnated with different lithium salts [11]

In this study, polymeric membranes were prepared based on polymer blend with inorganic particles. PVDF/PEO/AgNO<sub>3</sub> porous membranes were prepared by casting method. The effect of porous forming additives within a casting solution from PEO and Ag particles on the properties of membranes was investigated by different techniques. Membranes morphology and performance were examined and compared with blank polymer membrane prepared in the same conditions but without any additives.

## EXPERIMENTAL

### Materials

Polyvinylidene fluoride (PVDF) with  $M_w = 180000$  was obtained from Aldrich (USA), polyethylene oxide (PEO) of molecular weight 900000 supplied from ACROS (New Jersey, USA) and silver nitrate (AgNO<sub>3</sub>) obtained from Sigma-Aldrich Company.

### Preparation of PVDF/PEO porous membranes

Porous membranes of PEO/PVDF doped AgNO<sub>3</sub> were prepared by casting method as the following. PVDF and PEO were dried in oven for 4 h at 70 °C to remove moisture content. Various ration of PEO/PVDF (0.5/95.5, 1/99, 2.5/97.5, 5/95 and 10/90 wt./wt.) with constant concentration of AgNO<sub>3</sub> (10 wt.%) were dissolved in dimethyl sulfoxide (DMSO) at to prepare

porous membranes. The pH value of solutions was adjusted at 4 by aqueous solution of  $\text{HNO}_3$ . Resulting homogeneous solutions were cast on a Petri dishes, left to dry in oven at  $70^\circ\text{C}$  under vacuum about 3 days to form the desired film and then the film was stripped from the dish. The prepared membranes were kept in vacuum desiccators until use.

### Measurement techniques

The X-ray diffraction scans were obtained using DIANO corporation-USA equipped using  $\text{Cu-K}_\alpha$  radiation ( $\lambda=1.540 \text{ \AA}$ , the tube operated at 30 kV, the Bragg angle ( $2\theta$ ) in the range of  $5\text{--}60^\circ$ ). FT-IR absorption spectra were obtained using single beam Fourier transform-infrared spectrometer (FT-IR-430, JASCO, Japan). FT-IR spectra of the samples were obtained in the spectral range of  $2000\text{--}400 \text{ cm}^{-1}$ . UV-visible absorption spectra were measured in the wavelength region of  $190\text{--}1000 \text{ nm}$  using spectrophotometer (V-570 UV-VIS-NIR, JASCO, Japan). Scanning electron micrographs was obtained using SEM (JEOL-JSM 6100), operating voltage at 30KV accelerating voltage. Differential scanning calorimetry was carried out using (DSC-50, Shimadzu, Japan) with measuring temperature range from room temperature up to  $210^\circ\text{C}$  with heating rate was  $10^\circ\text{Cmin}^{-1}$ . A Perkin-Elmer TGA-7 was used for thermogravimetric analysis of membranes. The TGA was used to characterize the decomposition and thermal stability of prepared samples. The mass of the samples (amount  $1.2\text{--}2.8 \text{ mg}$ ) was recorded while temperature is increase at a heating rate of  $10^\circ\text{Cmin}^{-1}$  and the samples heated from room temperature to  $550^\circ\text{C}$ .

## RESULTS AND DISCUSSION

### X-ray diffraction analysis

Figure 1 represent X-ray diffraction (XRD) scans for pure PVDF with different content of PEO films doped with 10 wt%. of  $\text{AgNO}_3$ . It is seen that the peaks at  $2\theta = 18.12^\circ$  (020) and  $38.51^\circ$  (002) for  $\alpha$ -phase, at  $2\theta = 20.51^\circ$  (110 or 200) and  $35.84^\circ$  (001) for  $\beta$ -phase and at  $2\theta = 26.38^\circ$  (022) for  $\gamma$ -phase [12-15]. In all membranes there are mainly two small peaks occurring at diffraction angle ( $2\theta$ ) of  $12.7^\circ$  and  $30.25^\circ$  corresponding to (120) and (112 or 004) reflections from PEO crystallites [16, 17]. It is clear that intensities of PVDF peaks decreased monotonically with increase of PEO content and such observations seem to suggest a simple mechanism for decrease of crystallinity. Sharp peak at  $2\theta = 10.01^\circ$  is attributed to Ag which has a constant for all membranes (the amount of  $\text{AgNO}_3$  is a constant for the membranes). Behavior of dominant crystalline phase after adding PEO and  $\text{AgNO}_3$  can be also predicted from figure 1 in order to indicate the change in dominant crystalline phase.

The degree of crystallinity ( $\chi$ ) was estimated as ratio of the area under crystalline peak at  $2\theta = 20.51^\circ$  to the total area under halo peaks including that due to PEO. Both intensity and crystallinity are slightly decreased as a result of complexation between PVDF and PEO which reflected by polymer chain crystal. These decreasing are noticed significantly with increasing PEO contents.

## Fourier transform infrared analysis

Figure 2 shows FT-IR absorption spectra for pure PVDF and PVDF doped with 0.5, 1, 2.5, 5 and 10 wt.% of PEO with 10 wt.% of AgNO<sub>3</sub> respectively. Beside X-ray technique FT-IR could be used also to confirm occurrence of PVDF-phases; most bands of PVDF-phases are noticed. Bands at 532, 615, 763, 796, 975 and 1070 cm<sup>-1</sup> are corresponded to  $\beta$ -phase, whereas the band at 510 cm<sup>-1</sup> is a result of  $\gamma$ -phase of PVDF while at 487, 839 and 876 cm<sup>-1</sup> are belonging to  $\gamma$ -phase. Bands at 532 and 839 cm<sup>-1</sup> were assigned to CF<sub>2</sub> bending and at 615 and 796 cm<sup>-1</sup> were assigned to CF<sub>2</sub> bending and skeletal bending vibrational mode. Bands at 763, 796 and 839 cm<sup>-1</sup> are attributed to CH<sub>2</sub> rocking, at 975 cm<sup>-1</sup> is assigned to CH out of plane deformation and bands at 876 and 1070 cm<sup>-1</sup> are a result of CF<sub>2</sub> symmetric stretching and CH<sub>2</sub> wagging mode respectively. Furthermore, strong absorbance at 1170 cm<sup>-1</sup> was resulted from stretching vibration of CF [18, 19]. Spectra of membrane films after adding PEO and AgNO<sub>3</sub> have some changes in band intensities and band positions (shift) as compared with the spectrum of pure PVDF. This confirms the interaction between PVDF and PEO takes place. Then the interface microvoids may be produced due to a good miscibility in PEO/PVDF/AgNO<sub>3</sub> membrane films.

FT-IR spectra of resulting membrane indicated that the stretching vibration band at 1107cm<sup>-1</sup> was disappeared. This is attributed to specific interaction between fluorine in PVDF and carbon connected to oxygen of PEO, the fluorine in PVDF and carbon in PEO. Characteristic bands of PEO at 1230 and 1275 cm<sup>-1</sup> due to C-O and C-O-C bonding were observed respectively [20]. Intensities of absorbance bands at 839 and 876 cm<sup>-1</sup>, belonging to  $\gamma$ -phase of PVDF. These bands were increased with increasing PEO contents. It is worth to mention that  $\gamma$ -phase is the most important phases due to their high polarizability and it is useful in electrical applications since PVDF is a piezoelectric polymer [21].

## UV-Vis studies

UV-vis spectra in wavelength range of 190-1000 nm of all membranes at room temperature are recorded and plotted as shown in Figure 3. The presence of absorption edge at about 276 nm has small shift toward longer wavelengths with increasing PEO as indicated in Table 1. This indicating the complexation between all used components and may be attributed to change in crystallinity. The absorption shoulder centered in the range from 280 to 312 nm may be attributed to  $\pi \rightarrow \pi^*$  transitions which comes from unsaturated bonds, mainly; carbonyl groups (C=O and/or C=C). Another broad band centered at 420 nm can be assigned to Ag, where its intensity is a constant with increasing PEO.

The absorption coefficient ( $\alpha$ ) was calculated from the spectra using the formula:

$$\alpha = 2.303 \times \frac{A}{d} \quad (1)$$

where  $A$  is the absorbance and  $d$  is the thickness of the sample.

Thutpalli and Tomlin derived an expression relating absorption coefficient ( $\alpha$ ) to photon energy ( $h\nu$ ) [22] as:

$$\alpha = A(h\nu - E_g)^n / h\nu \quad (2)$$

where,  $E_g$  is optical energy gap,  $A$  is a constant,  $h$  is Planck's constant and  $n$  is a number which characterizes the optical absorption coefficient processes. Its values for different types of transitions are as follows:  $n=1/2$ : direct allowed transition;  $n=2$ : indirect allowed transition. Both direct and indirect transitions occur and can be observed by plotting  $(\alpha h\nu)^2$  and  $(\alpha h\nu)^{1/2}$ , respectively, as a function of energy ( $h\nu$ ) as shown in Figures (4, 5). The extrapolation of the straight line regions onto x-axis gives an estimation of both direct optical energy ( $E_{gd}$ ) and indirect optical energy ( $E_{gi}$ ) depending the change of PEO contents which tabulated in Table 1. The values of band gaps ( $E_{gd}$  and  $E_{gi}$ ) were increased with increasing PEO and  $\text{AgNO}_3$ . This variation could be attributed to formation of defects in the membranes due to decrease in both of degree of crystallinity and increase of the amorphosity (change of the structure).

Moreover, all spectra are characterized by an exponentially decay tail at low energy indicating the presence of localized states in energy band gap. Also, figures (4, 5) show two distinct linear parts. This indicates that the allowed transitions are predominant in the optical absorption processes.

## SEM

During casting process, an exchange of solvent and nonsolvent in mixed phases continues to cause concentrated phase surrounding the porous. It was found that membranes have symmetrical morphology which are strongly affecting the structure which could be followed by SEM. Membrane pore size is an important factor to evaluate membrane separation performance. Pictures depict pore size was distributed in range from 0.10 to 0.65  $\mu\text{m}$  and centralized pore size of 0.15~0.3  $\mu\text{m}$ . Increasing of PEO can decreased pore size of the membranes. Figure 6 represents SEM images of the surfaces of pure PVDF (image a) and images (b-e) for 0.5, 1.0, 2.5 and 5 wt.% of PEO with 10 wt.% of  $\text{AgNO}_3$ . Image f represents the cross section of 0.5 wt.% of PEO with 10 wt.% of  $\text{AgNO}_3$ .

Pure PVDF membrane (picture a) has a rougher outer surface without obvious pores with spherulitic morphology. Additive of PEO and  $\text{AgNO}_3$  inducing enhancement of the membranes, increase the viscosity and delay mutual diffusion between solvent in coagulation bath and nonsolvent therefore, they induce a phase separation delay. Systems with a slow phase inversion rate tend to form macrovoids with a sponge-like structure.

The average pores size in the bottom surface is much larger than that of the upper surface. Centre of the porous sponge-like structures are possessed which formation of larger cavity structures. Moreover, as PEO content increases up to 5 wt.%, the micro pores become smaller and skin layer becomes thinner. The result is due to addition of PEO improving diffusion. It is evident that there is no big change in membrane morphology after adding 5 wt.% of PEO. All membranes have uniform distribution and aggregation of  $\text{AgNO}_3$  particles.

The porosity ( $P$ ) is determined by immersing membrane films into n-butanol for 1h, weighing the mass of samples with and without n-butanol and then determines the porosity using the following relationship [23]:

$$P = \frac{m_a / \rho_a}{m_a / \rho_a + m_p / \rho_p} \quad (3)$$

where  $m_a$  is film weight after impregnation with *n*-butanol,  $m_p$  dried film weight,  $\rho_a$  and  $\rho_p$  are densities of *n*-butanol and dried film, respectively. As shown in Table 1, the values of porosity are decreased dramatically from 0.43 to 0.07 after adding PEO.

### Differential scanning calorimetry

DSC thermograms of the prepared membranes over temperature range of 40–220 °C at a heating rate of 10 °Cmin<sup>-1</sup> under argon atmosphere are depicts in Figure 7. Observed thermal transitions can be assigned as follows: Broad exothermic peak ( $T_w$ ) is observed between 50 to 88 °C could be due to moisture. A sharp endothermic peak is observed at  $\sim 166 \pm 5$  °C assigned to melting temperature ( $T_m$ ). It is clear that, the melting temperature of the membranes is decreased dramatically with increase of PEO contents from 171.71 °C to 160.87 °C suggests a large influence of intercalation treatment of membranes matrices.

Some curves showed double melting peaks in DSC thermograms. The origin of these double melting peaks of semicrystalline polymers can be attributed to: i) polymorphism of polymer; ii) melting, recrystallization, and remelting during DSC heating; and iii) variation in morphology (like: lamellar thickness or perfection of crystals).

At melting peak it is possible to evaluate the degree of crystallinity. By assume that PVDF crystal form present has the same heat of fusion  $\Delta H_c \sim 104.7$  J/g for completely crystalline PVDF sample (100% crystalline) [24-27], then  $\Delta H_f$  (measured directly from DSC thermograms) can be related to relative percentage of crystalline ( $\chi_c$ ) of membranes as:

$$\chi_c \% = \frac{\Delta H_f}{\Delta H_c} \times 100 \quad (4)$$

The values of both melting temperature and the degree of crystallinity of all membranes are recorded in Table 2. Both of  $T_m$  and  $\chi_c$  are decreased with increasing of PEO content related to a good miscibility and homogeneity between PVDF, PEO and Ag.

### Thermogravimetric Analysis

Thermograms of membranes are shown in Figures 8. Characteristic degradation temperatures and its parameters obtained from these thermograms are summarized in Table 2.  $D_{10}$ ,  $D_{50}$  and  $D_{90}$  indicate temperature at 10%, half decomposition and 90% of decomposition occurs, respectively. Also, thermograms revealed the following regions of weight loss. Stage I up to 368 °C could be attributed to evaporate of moisture, CO and CO<sub>2</sub>; stage II from 380 to 480 °C attributed to the main degradation temperature of the membranes.

Usually the change in extent of reaction ( $\alpha$ ) is used to study of solid state reaction kinetic as:

$$\alpha = \frac{m_i - m_t}{m_i - m_\infty} \quad (5)$$

where  $m_i$ ,  $m_t$  and  $m_\infty$  are initial sample mass, sample mass at temperature  $t$  and sample mass at the end of reaction, respectively.

The activation energy for thermal decomposition for TGA measurements of present samples which depends on the residual mass can be calculated (non-isothermal kinetic method) using integral method at both of the first order of reaction and constant heating rate ( $10 \text{ }^\circ\text{Cmin}^{-1}$ ), The Coats and Redfern equation, based on mathematical approximations is [28]:

$$\ln\left[\frac{-\ln(1-\alpha)}{T^2}\right] = \ln\left[\frac{AR}{\Delta E}\left(1 - \frac{2RT}{E}\right)\right] - \frac{E}{RT} \quad (6)$$

where  $T$  is the absolute temperature,  $E$  is the activation energy in J/mol,  $R$  is universal gas constant ( $8.3136 \text{ J/mol K}$ )

Plotting the quantity on left hand side of the above equation versus inverse temperature ( $1/T$ ) for each sample and for progressing values of conversion ( $\alpha$ ) will result in a straight line which represented in Figure 9. The slope equals  $-E/R$  thus the values of activation energy ( $E$ ) can be determine. The activation calculated energies with this method are tabulated in Table 2, which varies from 199.93 to 271.92 KJ/mole. This is attributed to different components of PEO, Ag and their different decomposition mechanisms. The variation denotes changes in reactivity as a result of extent of reaction and the complex nature of the reaction.

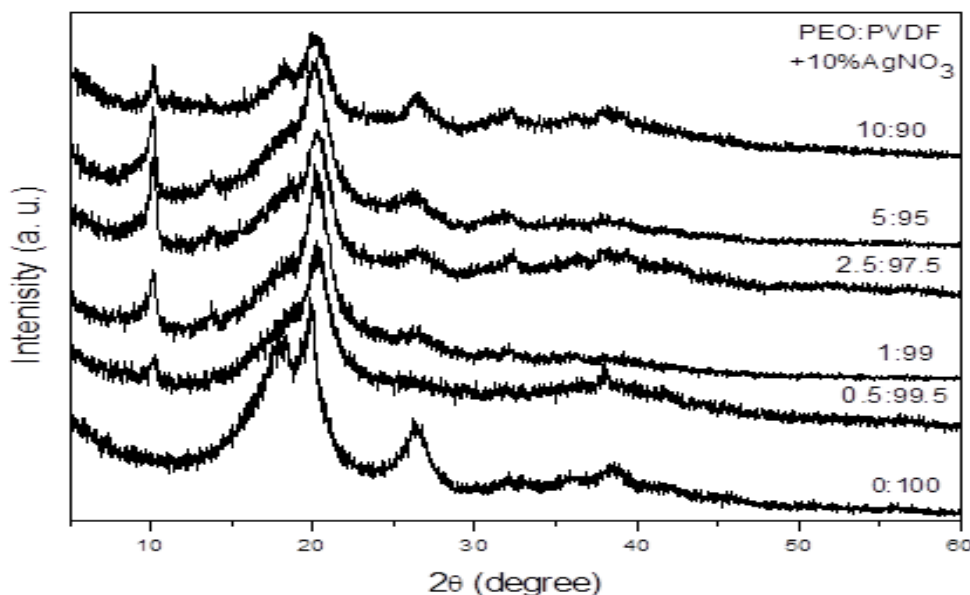


Figure 1: X-ray diffraction of pure PVDF and PVDF with different concentrations of PEO membranes with 10 wt.% of  $\text{AgNO}_3$ .

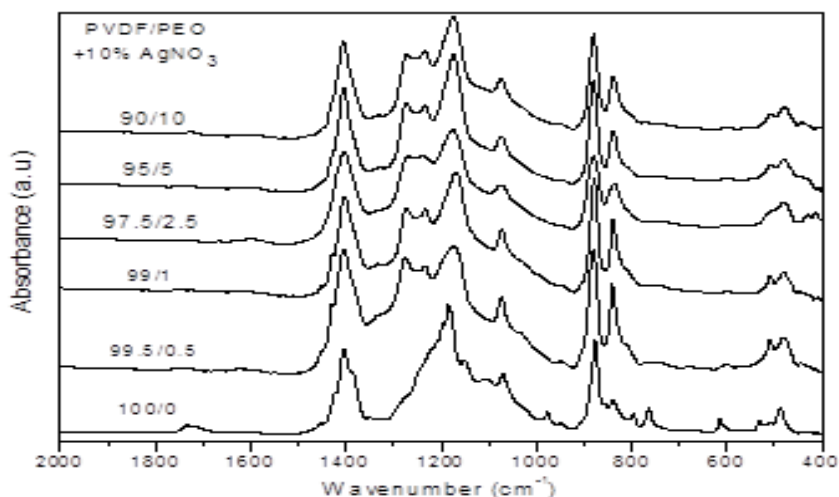


Figure 2: FTIR absorption spectra of pure PVDF and PVDF doped with 0.5, 1, 2.5, 5 and 10 wt.% of PEO with 10 Wt.% of AgNO<sub>3</sub>.

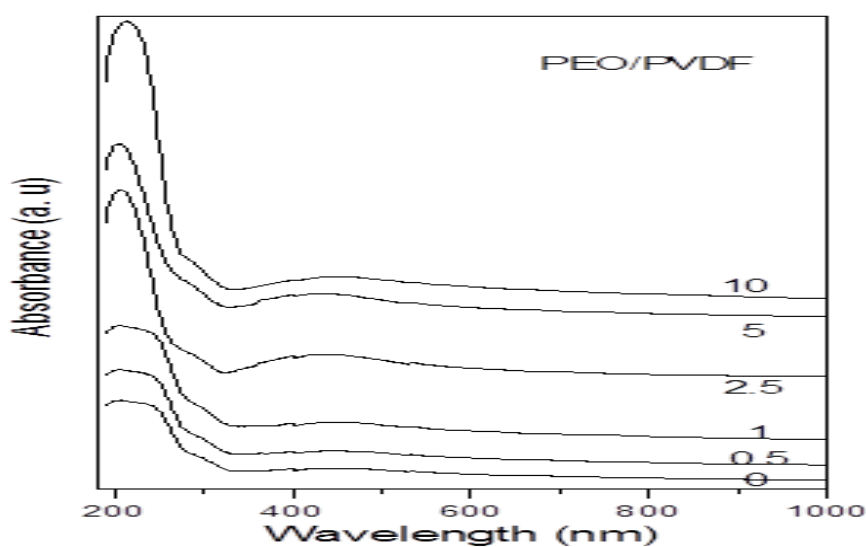


Figure 3: UV-vis spectra in the wavelength range of 190-1000 nm of pure PVDF and PVDF with different concentrations of PEO membranes with 10 wt.% of AgNO<sub>3</sub>.

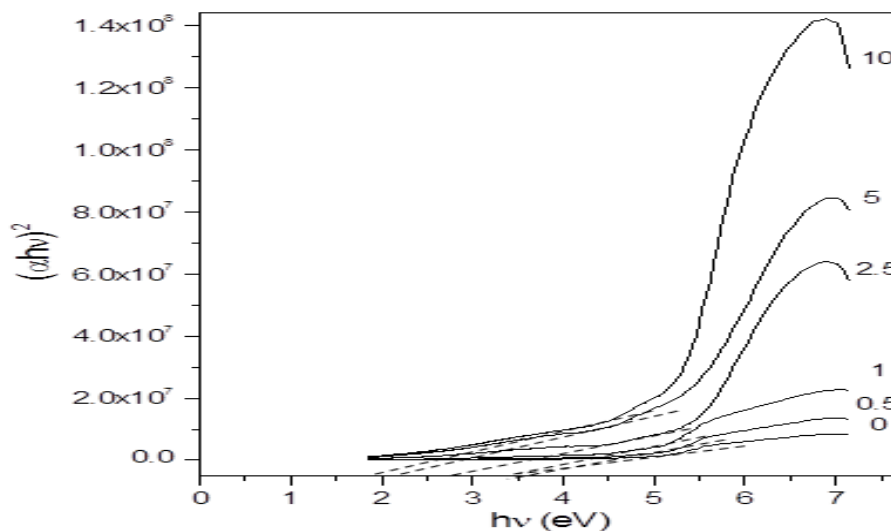


Figure 4:  $(\alpha h\nu)^2$  vis  $h\nu$  of pure PVDF and PVDF with different concentrations of PEO membranes with 10 wt.% of AgNO<sub>3</sub>.

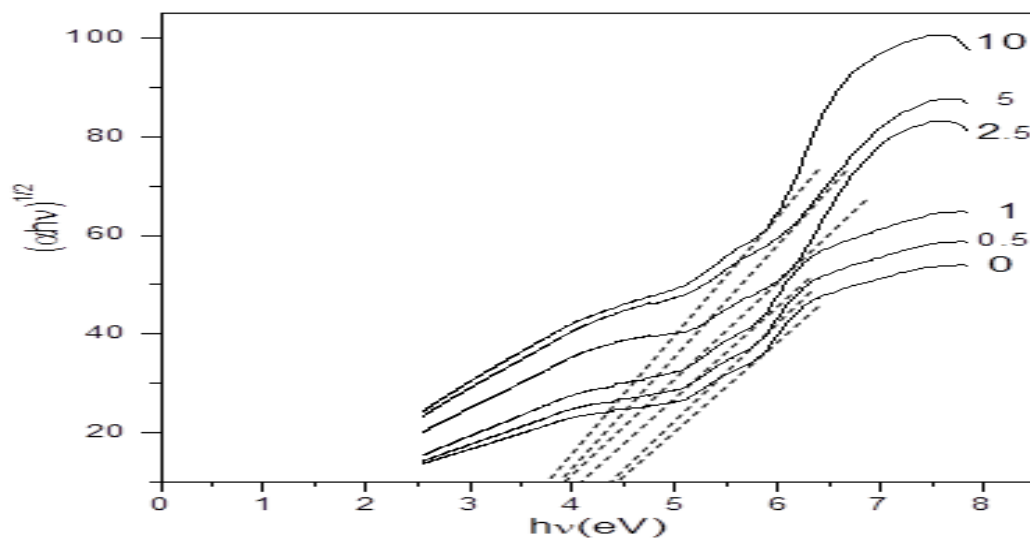


Figure 5:  $(\alpha h\nu)^{1/2}$  vis  $h\nu$  of pure PVDF and PVDF with different concentrations of PEO membranes with 10 wt.% of  $\text{AgNO}_3$ .

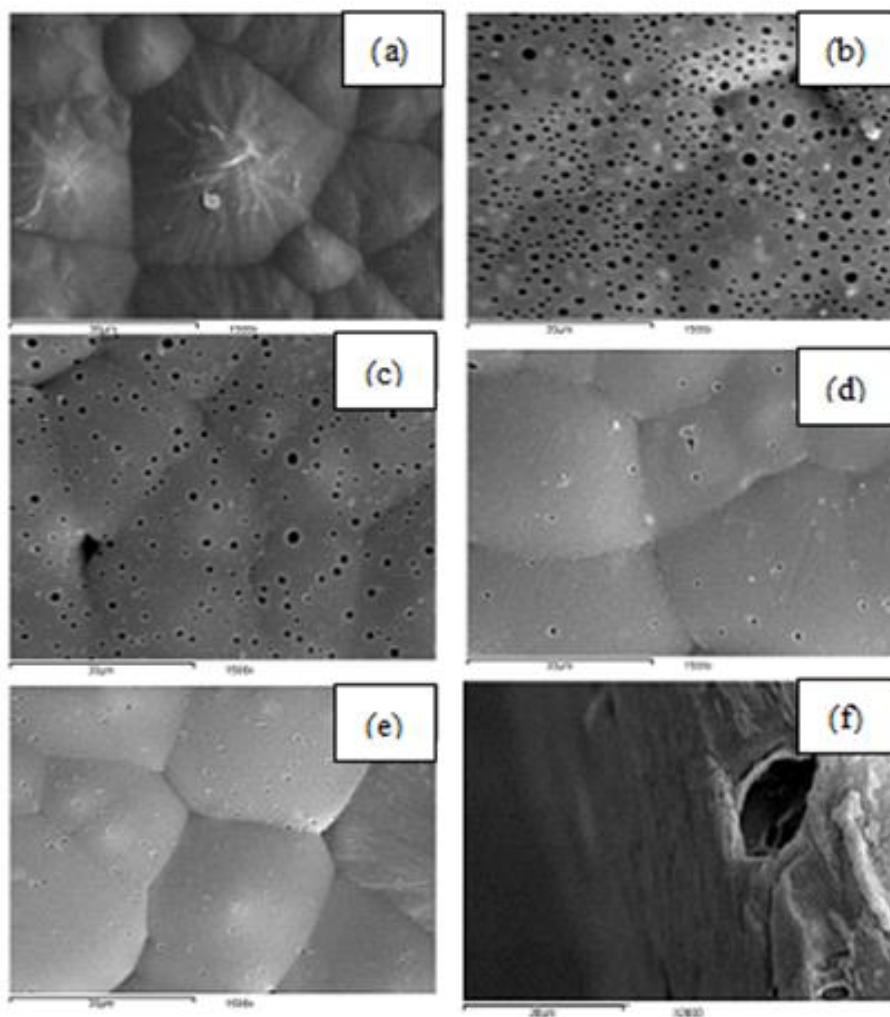


Figure 6: SEM images of the surfaces of (a) pure PVDF and PVDF with (b) 0.5 wt.% (c) 1wt.% (d) 2.5 wt.% and (e) 5 wt.% of PEO membranes with 10 wt.% of  $\text{AgNO}_3$  and (f) cross section of 0.5 wt.%.

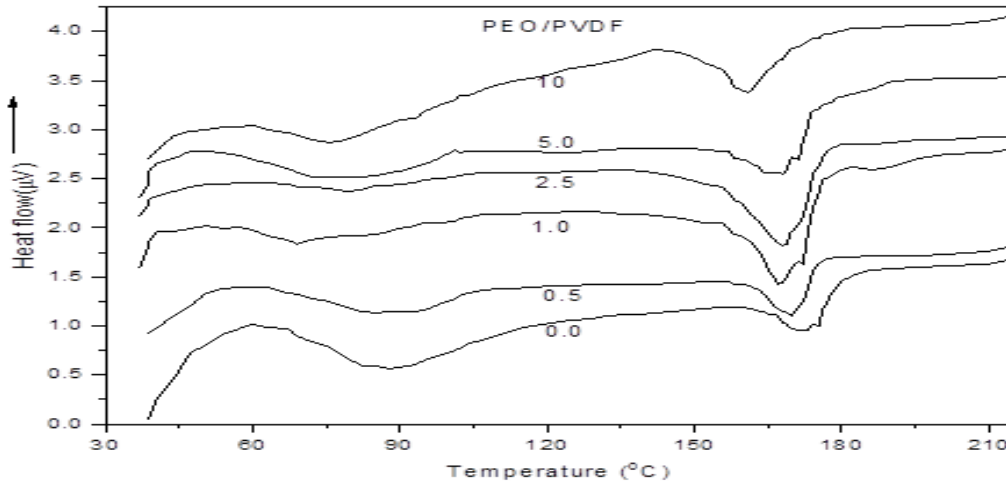


Figure 7: DSC thermograms of pure PVDF and PVDF with different concentrations of PEO membranes with 10 wt.% of AgNO<sub>3</sub>.

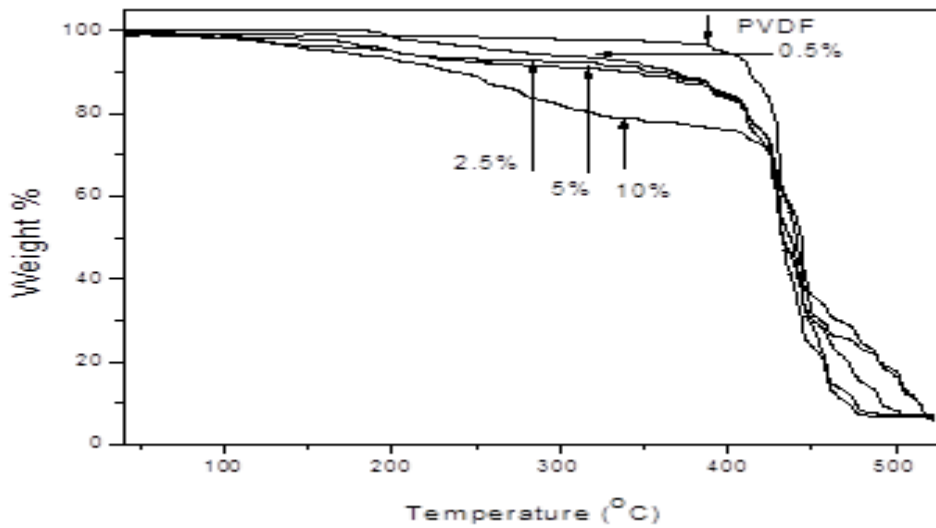


Figure 8: TGA thermograms of pure PVDF and PVDF with different concentrations of PEO membranes with 10 wt.% of AgNO<sub>3</sub>

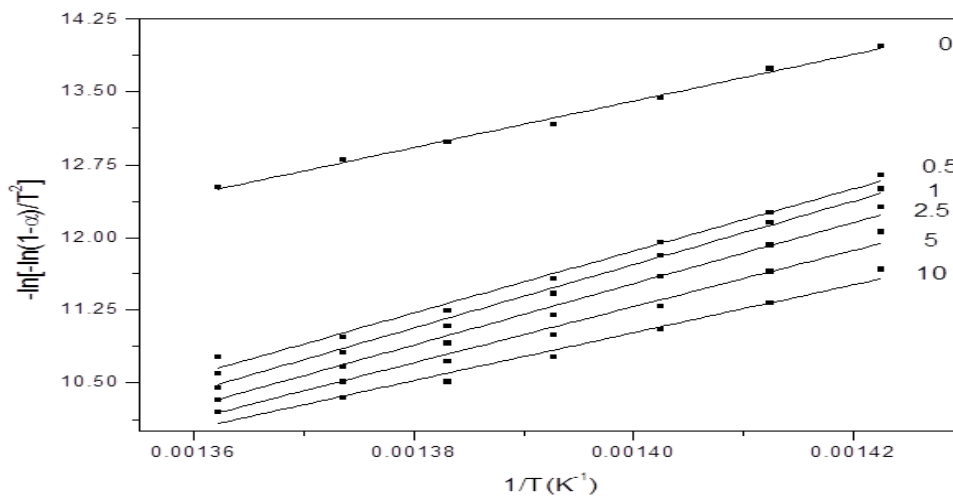


Figure 9: Plotting  $-\log\left[\frac{-\log(1-\alpha)}{T^2}\right]$  against  $1000/T$  (K<sup>-1</sup>).

**Table 1: Values of absorption edge, band energy gap and porosity of the membranes system.**

PEO/PVDF (wt.%)	Absorption edge (eV)	Band energy gap (eV)		Porosity%
		direct	indirect	
0.0	285	1.02	4.30	-
0.5	280	1.70	4.35	0.43
1.0	275	2.50	4.45	0.35
2.5	272	4.52	4.60	0.21
5.0	270	5.00	4.71	0.14
10	260	5.08	4.82	0.07

**Table 2: Values of melting temperature, degree of crystallinity and activation energy.**

PEO/PVDF (wt.%)	melting temperature (°C)	crystallinity %	decomposition temperature (°C) at different weight loss			Activation energy (J/mol.K)
			D <sub>10</sub>	D <sub>50</sub>	D <sub>90</sub>	
0.0	171.87	49.22	410	493	513	199.93
1.0	170.73	48.81	365	433	491	265.96
2.5	169.65	48.63	344	432	476	271.93
5.0	168.22	43.15	292	428	487	262.64
10	161.87	39.24	244	431	513	240.80

## CONCLUSIONS

PEO/PVDF membranes doped AgNO<sub>3</sub> were synthesized by casting method and characterized by spectroscopic techniques. XRD indicates that main characteristic peaks of two polymers were observed. Intensities of PVDF peaks decreased monotonically with increasing of PEO content. FT-IR spectra indicated that stretching vibration band at 1107cm<sup>-1</sup> was disappeared attributed to specific interaction between fluorine in PVDF and carbon connected to oxygen of PEO. Band intensity which belonging to  $\gamma$ -phase of PVDF was increased, this band is useful in electrical applications due to the polarizability (PVDF is piezoelectric polymer). Optical absorption edge and optical band gaps showed a decreasing trend with increase concentration of additions. Pore size and the porosity were decreased with increase of PEO with 10 wt.% of AgNO<sub>3</sub>. DSC thermogram reveals two regions of weight loss. The first region was attributed to evaporation of moisture and gases but the second one attributed to main degradation temperature. Variation of activation energies was attributed to decomposition mechanism and denotes changes in reactivity as a result of extent of reaction and complex nature. Values of melting and crystallinity of all membranes were decreased due to a good compatible, miscibility and homogeneity between all components.

## REFERENCES

- [1] L Yan Y S Li C B Xiang and S. Xianda J. Membr. Sci. 276 162 (2006).
- [2] I S Chang C M Chung and S H Han Desalination 133 225 (2001).
- [3] I S Elashmawi E M Abdelrazek H M Ragab and N.A.Hakeem Physica B: 405 94 (2010).
- [4] I. Elashmawi Cryst. Res. Technol. 42 389 (2007).
- [5] J R Gregorio J. Appl. Polym. Sci. 100 3272 (2006).

- [6] X Chen et al. Polym. Compos. 342 457 (2013).
- [7] G Kang and Y Cao J. Memb. Sci. 463 145(2014).
- [8] F Bossard N El Kissi A D'Apria F Alloin J Y Sanchez and A Dufres Rheol. Acta 49 529 (2010).
- [9] M Deka A K Nath and AKumar Indian J. Phys. 84 1299 (2010).
- [10] L Yue M Zhou Q Chen J Weng and Y Zhang Vacuum 83 1200 (2009).
- [11] V Aravindan and P Vickraman Indian J. Phys. 86 431 (2012).
- [12] Y Wang J. Wang F Wang S Li and J Xiao Polym. Bull. 60 647 (2008).
- [13] W Ma J Zhang S Chen and X Wang Colloid Polym. Sci. 286, 1193 (2008).
- [14] P Periasamy et al. Ionics 8 453 (2002).
- [15] P Vickraman V Aravindan M Selvambikai and N Shankarasubramanian Ionics 15 433 (2009).
- [16] M D Mihaylova V P Kretev M N Kreteva A Amzil and I V Berlinova Eur. Polm. J. 37 233 (2001).
- [17] A Chandra Indian J. Phys. 87 643 (2013).
- [18] Y Seo S M Hong and H J Choi Int. J. Mater. Form. 2, 869 (2009).
- [19] E. Adem et al. Bull. 52, 163 (2004).
- [20] Y Fang X Zhu D Yan Q Lu and P Zhu Collid Polym. Sci. 280 54 (2002).
- [21] Y Ahn J Y Lim S M Hong J Lee J Ha H J Choi and Y Seo J. Phys. Chem. C 117 11791 (2013).
- [22] C V S Reddy Q Y Zhu L G Mai and W Chen J. Appl. Electrochem. 36 1051 (2006).
- [23] M Gu J Zhang X Wang H Tao and L Ge Desalination 192 160 (2006)
- [24] D Wang K Li and W K Teo J. Membr. Sci. 178 13 (2000).
- [25] C Chiang M J Reddy and P P Chu Solid State Ionic 175 631 (2004).
- [26] Y Wang and D Kim Electrochimica Acta 52 3181 (2007).
- [27] K Nakagawa and Y Ishada J. Polym. Sci Polym. Phys. Ed. 11 2153 (1973).
- [28] A W Coats and J P Redfern Nature 201 68 (1964).